Theor. Comput. Fluid Dyn. (2015) 29:55–65
DOI 10.1007/s00162-015-0341-1

ORIGINAL ARTICLE

David Murphy · Xuerui Mao

Suppression of vorticity in vortex and pipe flow interactions

Received: 24 July 2014 / Accepted: 12 January 2015 / Published online: 28 January 2015

Abstract The interaction of a vortex and a pipe flow, modelled as the Lamb–Oseen vortex and the Poiseuille flow, respectively, is investigated by means of stability analyses and direct numerical simulations (DNS). From the distribution of the most unstable mode, it is observed that the instability is induced by the combination of the radial gradients of the base azimuthal and axial velocity components, e.g. an axial (or azimuthal) vorticity perturbation acts on the axial (or azimuthal) base velocity via a lift-up effect to generate axial (or azimuthal) velocity streaks, which are further stretched by the base azimuthal (or axial) velocity to create azimuthal (or axial) vorticity. This lift-up-stretch mechanism is confirmed in DNS of the model base flow initially perturbed by the most unstable mode. After nonlinear saturation, the perturbations decay since the flow no longer supports instability after sufficient radial mixing induced by the lift-up of the azimuthal and axial velocity components. These observations suggest that the vorticity outside the vortex core can be suppressed by instabilities if a streamwise boundary layer flow exists outside the core.

Keywords Vortex flow · Instabilities · Lift-up mechanism

1 Introduction

Vortex dynamics, e.g. stabilities and breakdown, have been extensively studied both numerically and experimentally. However, most of the previous work has been based on vortex flow in the free-stream, and the interaction of vortices and boundary layers has been less discussed. The development of vortices in the wake of an aircraft at take-off and landing involves the interactions with the ground surface and has important safety applications [1]. The vortices are forced into the ground surface owing to the downwash effect, subsequently inducing boundary layer separation and the generation of secondary vortices with opposite vorticity [2]. This ground effect on vortex flow is ubiquitously observed, e.g. in the wake flow of road vehicles and wind turbines, and can be generalised as the interaction of boundary layers with vortices. Such an interaction can be studied in a pipe/vortex flow, which accommodates an azimuthally homogeneous interaction between the vortex and the boundary layer and is numerically easier to setup than the plane ground/vortex flow. Therefore a pipe geometry is adopted in this study. It is noticed that the stability and breakdown of vortex flow confined in a pipe have been well investigated, but the interaction of a vortex and an axial pipe flow has received limited attention [3,4].

In fluid stability analyses, an initial perturbation is added to a base flow to investigate the development of the perturbation using a linearised governing equation, i.e. the Navier–Stokes (NS) equation. If the base flow is homogeneous in two orthogonal directions, the perturbation can be Fourier decomposed in these two

Communicated by Peter Duck.

D. Murphy · X. Mao (✉)
School of Engineering and Computer Sciences, Durham University, Durham DH1 3LE, UK
E-mail: maoxuerui@sina.com; xuerui.mao@durham.ac.uk

directions, effectively reducing the stability calculation to be one dimensional and enabling analytical analyses of stabilities for given wavenumbers in the two directions. This "local" stability analysis has been extensively used in shear flow and vortex flow [5,6]. If the base flow is homogeneous in one direction, the perturbation can be decomposed in this direction, which reduces the stability calculation to be two dimensional. This "BiGlobal stability analysis" can be conducted using two-dimensional mesh for given wavenumbers in the homogeneous direction, as has been used in shear flow, pipe flow and vortex flow [7,8], and will be adopted in this work. For base flow that is inhomogeneous in all directions, a three-dimensional calculation is required and owing to the high requirement of computational resources, this approach has not been widely discussed [9].

For stabilities of vortex flow, several analytical models of an isolated vortex have been established and well studied, e.g. the Burgers vortex [3], the Long's vortex [10], the Batchelor vortex [11] and the Lamb–Oseen vortex [12]. The Lamb–Oseen vortex has zero axial velocity and can be regarded as the Batchelor vortex with an azimuthal velocity much stronger than the axial one. In this work, the Lamb–Oseen vortex is adopted so that in the pipe/vortex base flow, the axial and azimuthal velocity components are decoupled, with one specified from the pipe flow model and the other from the vortex flow model. In stability studies of an isolated vortex flow, three types of eigenmodes are identified: core modes, potential modes and free-stream modes [6]. The energy of core modes concentrates inside the vortex core and decays exponentially outside the core, potential modes exist in the region outside the vortex core and decay algebraically in the radial direction, and free-stream modes oscillate in the free-stream without any decay. The eigenmodes of perturbations to a vortex flow are highly non-normal, meaning that the sum of two decaying modes can grow transiently before eventually decaying. This transient energy growth has been extensively studied in the asymptotically stable Lamb–Oseen vortex flow and can be explained by an anti-lift-up mechanism [13], referring to energy transfer from the azimuthal velocity component to the azimuthal vorticity component, reported to be closely associated with the non-normality of the continuous modes [14]. The counterpart of this mechanism, that is the lift-up mechanism, referring to the energy transfer from axial vorticity to axial velocity in a boundary layer flow, has been exhaustively investigated and is known to be responsible for the generation of high- and low-speed axial velocity streaks [15,16].

The pipe flow model adopted in this work, i.e. the Poiseuille flow, is generally assumed to be asymptotically stable at Reynolds number $Re < 2{,}000$ [17], although the condition at which the laminar to turbulence transition begins is still an open question. The Reynolds number adopted in this work is well below the critical value and therefore the two models, the pipe flow and the vortex flow, are individually stable. These specifications isolate the individual instabilities from the coupling effects of the two models: any instabilities of the combined flow will be owing to the interaction of the vortex and the pipe flow.

2 Methodology of global stability analyses

This investigation assumes that the fluid is Newtonian and incompressible. In the cylindrical frame, where x, r and θ are the axial, radial and azimuthal coordinates, respectively, the governing equation, i.e. the NS equation, can be expressed as

$$\partial_t \boldsymbol{u} = -(\boldsymbol{u}\cdot\nabla)\,\boldsymbol{u} - \nabla p + \frac{1}{Re}\nabla^2\boldsymbol{u} \qquad \text{with} \qquad \nabla\cdot\boldsymbol{u} = 0$$

where $\boldsymbol{u}(x, r, \theta, t)$ is the velocity vector, $p(x, r, \theta, t)$ is the modified pressure, and Re is the Reynolds number. $Re = 1{,}000$ is used throughout this work, as has been widely adopted in the literature [14,18]. The pipe radius and the maximum axial velocity are used to define the Reynolds number. The stability analysis of a steady flow to perturbations is based upon the decomposition of the flow variables into a summation of a steady base flow field and a small-amplitude perturbation field (i.e. $\boldsymbol{u} = \boldsymbol{U} + \boldsymbol{u'}$). Neglecting the interaction of the perturbation with itself, the governing equation for the perturbation is the linearised NS equation:

$$\partial_t \boldsymbol{u} = -\left(\boldsymbol{u}'\cdot\nabla\right)\boldsymbol{U} - (\boldsymbol{U}\cdot\nabla)\boldsymbol{u}' - \nabla p' + \frac{1}{Re}\nabla^2\boldsymbol{u}' \qquad \text{with} \qquad \nabla\cdot\boldsymbol{u}' = 0 \tag{1}$$

Since the base flow adopted in this work is homogeneous in the axial direction, the perturbation can be decomposed as

$$\boldsymbol{u}'(x, r, \theta, t) = \hat{\boldsymbol{u}}(r, \theta)\exp(\mathrm{i}kx + \sigma t)$$

where $\hat{\boldsymbol{u}}$ is the eigenmode at axial wavenumber k with growth rate Real(σ) and frequency Imag(σ). Owing to the linearisation of the governing Eq. (1), developments of modes with different axial wavenumbers are

decoupled and can be studied separately. At a prescribed axial wavenumber, if all the eigenmodes have negative growth rates, the flow is asymptotically stable while if at least one eigenmode has a positive growth rate, the flow is unstable to initial disturbances. The most unstable mode (with the largest growth rate) can be calculated using an Arnoldi method, as has been extensively implemented in both pipe flow and vortex flow in BiGlobal stability and transient growth studies[14,19]. It is worth noting that the base flow is also homogeneous in the azimuthal direction, and therefore, the perturbation can be also decomposed in the azimuthal direction to enable a local analytical study. However, this local analysis is not implemented in this work, since the BiGlobal approach is more general, e.g. it can be also used to study the interaction of vortex and a plane boundary layer flow, and its numerical setup matches well with further nonlinear studies of the unstable modes in direct numerical simulations (DNS), as will be conducted in Sect. 6.

3 Base flow model

As stated above, the base flow model adopted in this work is a combination of two basic flows: a pipe flow and a vortex flow, which provide the axial and azimuthal velocity components of the base flow, respectively.

The pipe flow, i.e. the Poiseuille flow featuring a parabolic velocity profile in the axial direction, is defined as

$$U_x = 1 - r^2, \tag{2}$$

as illustrated in Fig. 1a. The pipe radius has been used as the length scale to non-dimensionalise r.

The vortex flow model, i.e. the Lamb–Oseen vortex, has zero velocity components in the axial and radial directions, and an azimuthal component defined as

$$U_\theta(r) = \frac{qR}{r}\left[1 - \exp\left(-\frac{r^2}{R^2 + 4t/Re}\right)\right], \tag{3}$$

where q quantifies the relative strength of the azimuthal (swirling) velocity compared with the maximum axial velocity in the pipe flow and R denotes the non-dimensionalised radius of the vortex. The axial vorticity generated by this azimuthal velocity profile is shown in Fig. 1b. It is worth noting that in the general definition of the Lamb–Oseen vortex, the swirling strength has unit value. However in this work, the radius of the pipe and the maximum axial velocity of the pipe flow have been used as reference values, and therefore, q is introduced to define the strength of the swirling velocity.

It is noticed that by setting the radial velocity to zero and neglecting the viscous diffusion, the velocity profiles defined by (2) and (3) at $t = 0$ form a steady solution of the NS equation, with pressure P satisfying $\mathrm{d}P/\mathrm{d}r = U_\theta^2/r$. Such a flow profile experiencing viscous decay at a finite Reynolds number has been widely used as a steady base flow in linear stability studies of vortex flow by freezing the profile at $t = 0$ [14,20,21], as will be also implemented in this work. The validation of this combined model flow as a solution of the NS equation is tested through two-dimensional (homogeneous in the axial direction) DNS, as illustrated in Fig. 2. In this calculation, the swirling strength and vortex radius are set to $q = 1$ and $R = 0.39$, respectively. It is noticed that the development of the azimuthal velocity obtained in DNS agrees very well with that predicted by (3).

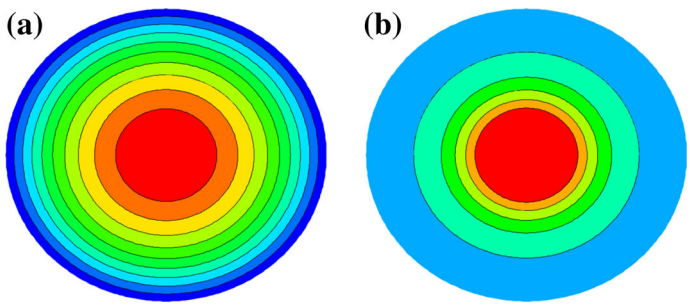

Fig. 1 Contours of the base flow. **a** Axial velocity with contour levels from 0.1 to 0.9 and **b** axial vorticity with contour levels from −0.4 to 2.6. The pipe radius has unit length. The vortex core and swirl strength are set to $R = 0.39$ and $q = 1$ respectively, which will be used in all the following figures and tables if not otherwise stated

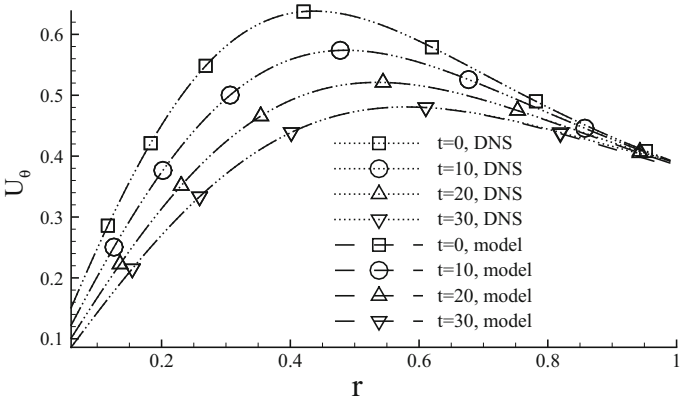

Fig. 2 Development of the azimuthal velocity component of the unperturbed base flow in two-dimensional DNS. The "model" results are obtained from Eq. (3). The Reynolds number is fixed at $Re = 1{,}000$ in this and all the following figures

Table 1 Convergence test of the growth rate of the most unstable mode with respect to the polynomial order $\mathcal{P}$ at axial wavenumber $k = 0.2$

$\mathcal{P}$	Real(σ)
2	0.044804
3	0.044808
4	0.044807
5	0.044807
6	0.044807
7	0.044806
8	0.044806

4 Convergence and discretisation

For both DNS and stability studies, a spectral/hp element method is used to discretise the NS and linearised NS equations. In this discretisation, the computational domain is decomposed into 1,679 spectral elements and each element is further decomposed into $\mathcal{P} \times \mathcal{P}$ smaller elements, where $\mathcal{P}$ is the polynomial order used in nodal expansion in each element. The convergence of the growth rate with respect to $\mathcal{P}$ at $R = 0.39$, $q = 1$ and $k = 0.2$ is presented in Table 1. It is seen that $\mathcal{P} = 4$ gives a relative error less than 0.003 % with respect to $\mathcal{P} = 8$ and is adopted all over this work in both stability analyses and DNS.

5 Flow instabilities

Dependence of the growth rate of the most unstable modes on the swirling strength q is shown in Fig. 3a. The vortex radius is fixed at $R = 0.39$, where the instability reaches maximum for the $q = 1$ case, as will be discussed later. It is seen that the growth rate almost increases monotonically with q and is not a smooth function with respect to the wavenumber k, but consists of several segments. Inspecting the structures of the unstable modes, it is observed that each segment corresponds to an azimuthal wavenumber (as the base flow is homogeneous in the azimuthal direction, each global mode calculated here has an azimuthal wavenumber), which increases with k. It is worth noting that at $q \leq 0.2$, the base flow becomes asymptotically stable. Considering that a large value of q requires more resolutions but reveals similar instabilities with a lower q, the swirling strength is fixed at $q = 1$ in the following analyses if not otherwise stated.

Figure 3b shows the growth rate at various vortex radius R. It is observed that there exists an optimal value of R, at which the growth rate reaches maximum. Zooming into the region $0.3 \leq R \leq 0.5$, this optimal value is found to be $R_{\text{opt}} = 0.39$. Above this optimal radius, the model is increasingly ill-defined, e.g. for $R = 1$, the vortex core fills all the domain and the vortex dynamics outside the vortex core is effectively truncated by the boundary. It will be presented later that the interaction of the out-of-core vortex flow with the boundary layer of the pipe flow is critical for the instabilities and therefore the growth rate reduces for $R > R_{\text{opt}}$. For

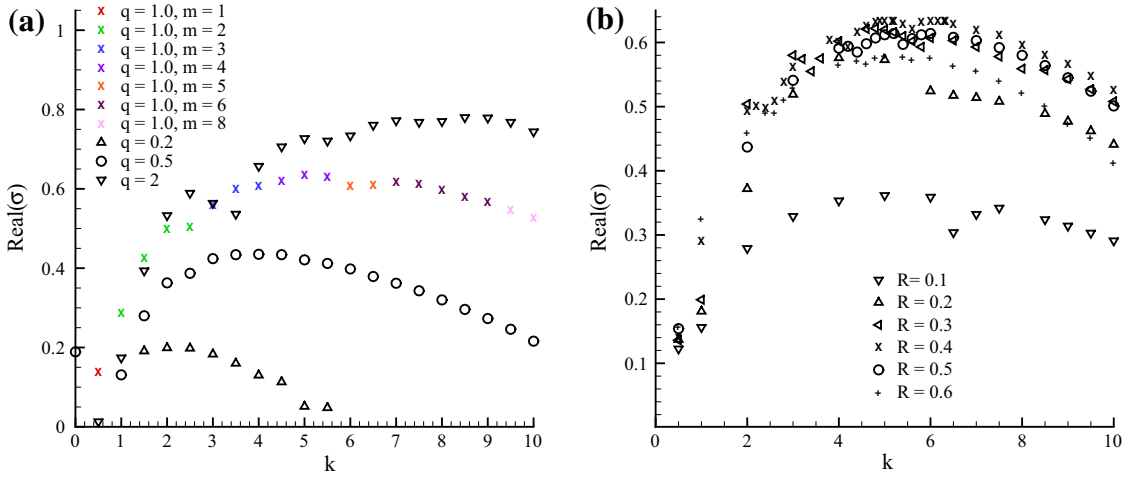

Fig. 3 Growth rates of the most unstable modes at **a** $R = 0.39$ and various q; **b** $q = 1$ and various R. In (**a**), the $q = 1$ case is further decomposed according to the azimuthal wavenumber of the mode, denoted as m

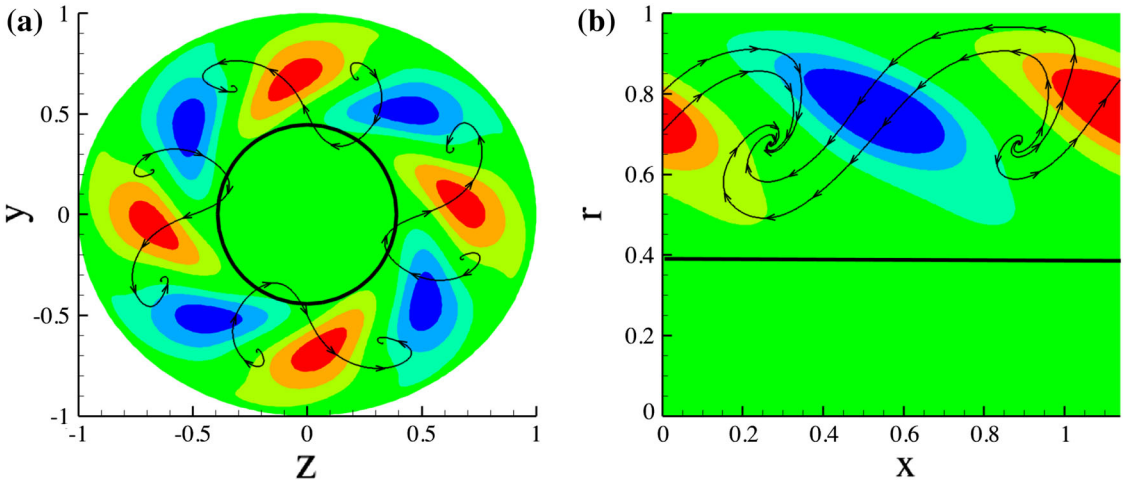

Fig. 4 Distribution of the most unstable mode at optimal streamwise wavenumber $k_{\text{opt}} = 5.1$, which has an azimuthal wavenumber $m = 4$. **a** Contours of the axial velocity on the $\theta - r$ plane, where $y = r\sin(\theta)$ and $z = r\cos(\theta)$, and **b** contours of the azimuthal velocity on the $x - r$ plane. The *thick lines* denote the vortex core $r = R_{\text{opt}} = 0.39$ and *arrow lines* denote streamlines of the mode

small values of the vortex radius, e.g. $R < R_{\text{opt}}$, the vortex and the pipe flow are decoupled, leading to a more stable model, since both the isolated Lamb–Oseen vortex and Poiseuille flow are stable.

In Fig. 3b, it is further noticed that the most unstable mode at $R = R_{\text{opt}}$ is obtained at an optimal wavenumber $k_{\text{opt}} = 5.1$. From Fig. 4, it is seen that the structure of this most unstable mode has an azimuthal wavenumber 4, with energy concentrated in the region between the vortex core and the wall boundary. This distribution is apparently different with the most unstable modes of a single vortex flow, which is concentrated inside the core [22]. It is noticed in Fig. 4a that all the positive (or negative) axial velocity perturbations are associated with positive (negative) radial velocity, suggesting that the perturbation is generated by radial convection of the base flow, whose axial velocity components are larger around the core and smaller around the wall boundary. Owing to the radial gradient of the base azimuthal velocity, the perturbation is stretched to tilt forwards around the core and backwards around the wall boundary. A similar distribution is observed in the axial direction from the contour of the azimuthal velocity perturbation on the $x - r$ plane, which is obtained in another set of BiGlobal stability calculations using axial domain size $2\pi/k_{\text{opt}}$ and azimuthal wavenumber 4, as shown in Fig. 4b. It is seen that the positive (negative) azimuthal velocity is associated with positive (or negative) radial velocity, which convects the base azimuthal velocity in the radial direction. Also the radial gradient of the base axial velocity stretches the perturbation to tilt forwards around the core and backwards around the wall boundary.

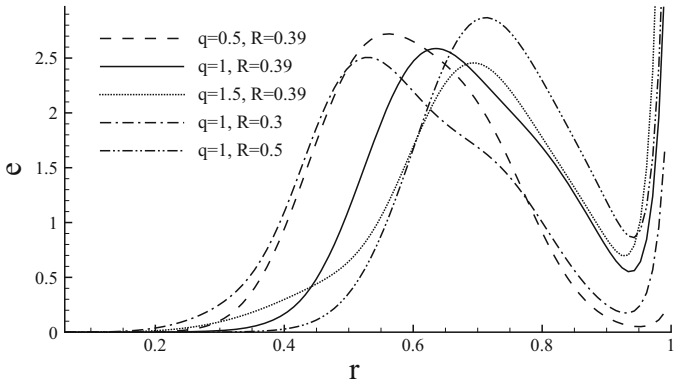

Fig. 5 Radial distribution of the energy of the most unstable modes at $k = 5.1$, which is averaged in the azimuthal direction and normalised

To better illustrate the radial distribution of the mode, the energy of the mode is averaged in the azimuthal direction and normalised, i.e. $e = \int_0^{2\pi} \hat{\boldsymbol{u}} \cdot \hat{\boldsymbol{u}} \mathrm{d}\theta / \int_0^1 (\int_0^{2\pi} \hat{\boldsymbol{u}} \cdot \hat{\boldsymbol{u}} \mathrm{d}\theta) \mathrm{d}r$, as shown in Fig. 5. It is observed that at higher values of q or R, which increase the radial gradient of the base azimuthal velocity and strengthen the stretching effect, the radial distribution of the mode energy becomes more concentrated and the peak moves outwards to the region with higher radial gradients of the base flow. This perturbation distribution and the associated instability mechanism will be discussed in detail in Sect. 7.

6 Nonlinear development of the most unstable modes

In this section, the nonlinear development of the unstable modes is studied through DNS. The initial condition is the model base flow perturbed by the globally most unstable mode at $q = 1$, which corresponds to an optimal vortex radius $R_{\mathrm{opt}} = 0.39$ and an optimal axial wavenumber $k_{\mathrm{opt}} = 5.1$. In these calculations, the axial domain length is set to $2\pi/k_{\mathrm{opt}}$ and 16 modes are calculated by implementing an axial Fourier decomposition [23,24]. The axial wavenumbers of these modes are 0, $2\pi/k_{\mathrm{opt}}$, $4\pi/k_{\mathrm{opt}}$, ..., $30\pi/k_{\mathrm{opt}}$, where the first, second and following ones will be noted as the base mode, leading mode and higher harmonic modes in the following. This numerical setup enables the free development of the perturbed base model and the nonlinear energy transfer between all the calculated modes without introducing inflow and outflow boundaries. The development of the mode will be evaluated by the kinetic energy, denoted as E and calculated as the square integration of the mode velocity over the domain.

In this nonlinear study, the magnitude or energy of the initial disturbance in the form of the most unstable modes has to be small to take advantage of the linear asymptotic growth. Three energy levels of the most unstable mode with respect to the base flow are considered, $f = 10^{-4}$, $f = 10^{-6}$ and $f = 10^{-8}$, respectively. Lower values of the initial energy are not studied since it would require a longer time to amplify the perturbation to reach the nonlinear stage, and the viscously diffusing base flow would have different amplification effects to perturbations after a long time decay. From Fig. 6a, it is seen that the perturbations experience an initial linear growth, followed by slower growth and nonlinear saturation. However, after the saturation, the perturbation decays instead of keeping the magnitude, as has been observed in many other unstable flows perturbed by unstable modes [18,25]. As can be expected, a higher initial perturbation energy results in maximum perturbation energy at earlier time and the value of the maximum energy is not sensitive to the initial perturbation level. It is seen that the higher harmonics follow the same trend of the leading mode, and energy decay is observed after the nonlinear saturation. The mechanism of this perturbation decay will be investigated later. The energy development of the base mode is shown in Fig. 6b. It is noticed that the unperturbed base mode decays almost linearly, while the perturbation induces a sharp drop of the base mode energy before the linear decay resumes at the same time of the decay of the leading mode. These results suggest that the base mode is changed dramatically by the perturbation over the first several time units and the modified base mode does not support the growth of the leading mode, resulting in the decay of the leading and higher harmonic modes.

In the following of this section, the energy level of the perturbation is fixed at $f = 10^{-6}$ to study the development of the flow pattern. From Fig. 6, it is seen that the modes reach a critical point at $t = 4.5$, where the base mode turns to linear decay and the leading mode and higher harmonics reach energy maxima.

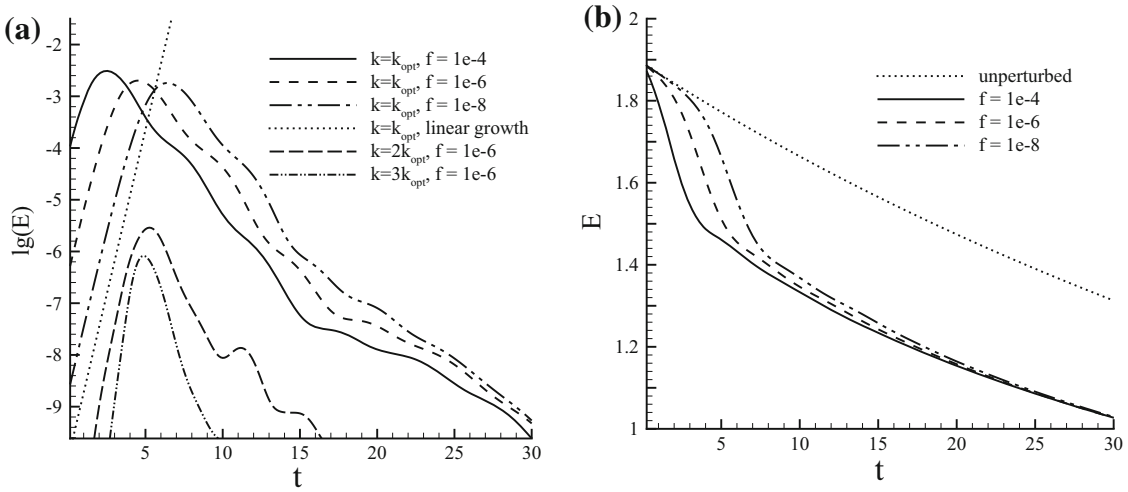

Fig. 6 **a** Energy of the leading mode with axial wavenumber $k = k_{\text{opt}} = 5.1$ and its higher harmonics and **b** energy of base modes at various perturbation levels. E denotes the kinetic energy, i.e. the square integration of the mode velocity over the domain

Therefore three time points are considered in the following, $t = 0$, $t = 4.5$ and $t = 20$, which are the initial, critical and a post-perturbed time points, respectively.

From the unperturbed development of the axial vorticity at $t = 0$, 4.5 and 20, as shown in Fig. 7a–c, respectively, it is seen that the unperturbed flow decays monotonically with time as has been observed in Fig. 6b. When the flow is perturbed by the unstable mode, the central region of the flow remains similar to the unperturbed case but the disturbance has created a spiralling of the flow with azimuthal wavenumber $m = 4$ (see Fig. 7d. At $t = 4.5$, the flow has reached its maximum energy and the vorticity field has completely changed. Regions of high vorticity have spread right out towards the boundary surface in four arms spiralling from the core. Between these arms, areas of negative vorticity have developed, where the perturbation has overcome the vorticity in the base flow to change its direction (see Fig. 7e). The form of the perturbation, with its azimuthal wavenumber $m = 4$, is now dominant and the flow has adopted its structure of alternate pairs of large positive and negative structures (Fig. 4). This structure creates high velocity gradients, which can be quickly diffused by viscous effects. Small parts of the near-wall region have also been taken over by high vorticity magnitudes. By $t = 20$, the spiralling arms of high vorticity and the regions of negative vorticity have decayed and the flow is dominated by the base mode with axial vorticity concentrated around the centre of the domain surrounded by a few remnants of the perturbation (see Fig. 7f). Over this development, the centre of the core region has been almost unaffected by the perturbation. The destruction of vorticity outside the centre results in decoupling of the vortex flow and the axial pipe flow. As discussed before, an isolated Lamb–Oseen vortex flow or a Poiseuille flow is asymptotically stable. Therefore this modified base mode does not support instabilities and perturbations start to decay at $t > 4.5$, as has been observed in Fig. 6a.

The 3D views of the perturbed flow at the three time points are presented in Fig. 7g–i through iso-surfaces of axial vorticity. The core structure can be seen to develop from a two-dimensional regular cylinder shape at $t = 0$ to a more angular three-dimensional core region with four large streams at $t = 4.5$ before it decays to a smaller, slower and almost two-dimensional structure at $t = 20$.

The azimuthal and axial velocity components are further averaged in the azimuthal and axial directions to illustrate the nonlinear development of the flow in the radial direction, as shown in Fig. 8. It is observed that before saturation, the high-speed azimuthal or axial velocity streaks are convected outwards, and vice versa, resulting in velocity reduction in the high-speed region around the core and velocity increase in the low-speed region around the wall boundary. After saturation, the velocity decays at both the core and wall boundary regions as has been observed in Fig. 7.

7 Mechanisms

In this section, the mechanisms of linear instability and the decay of perturbations after saturation in nonlinear developments will be investigated. For analysis' sake, notation is used to split the flow into three regions: A

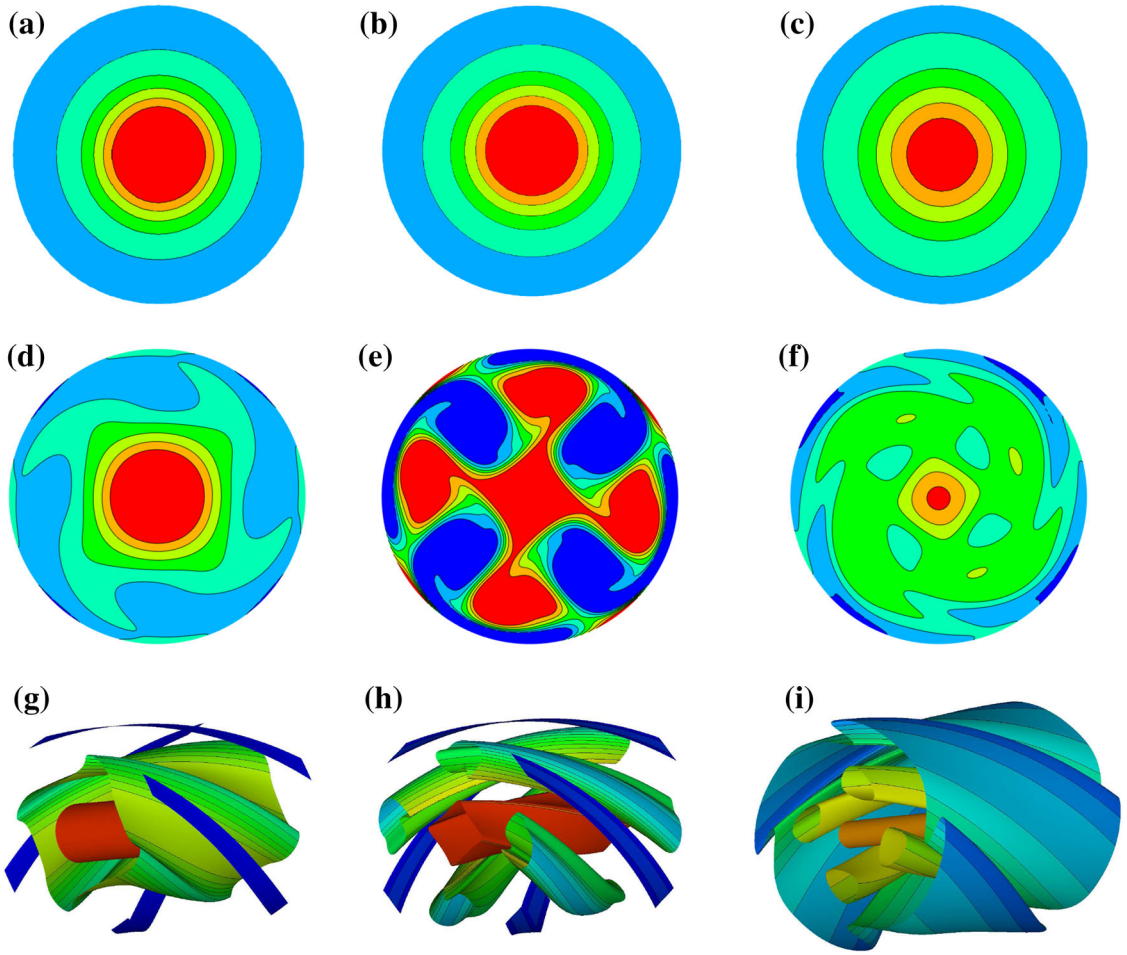

Fig. 7 Development of the axial vorticity at $t = 0$, 4.5 and 20 from left to right. **a–c** and **d–f** contours of the unperturbed and perturbed flow respectively, with contour levels ranging evenly from -0.4 to 2.6; **g–i** iso-surfaces of $\tau_x = 3$ and $\tau_x = 0.5$ (only $\tau_x = 3$ is shown in **h** for clarification) of perturbed flow coloured by the axial velocity

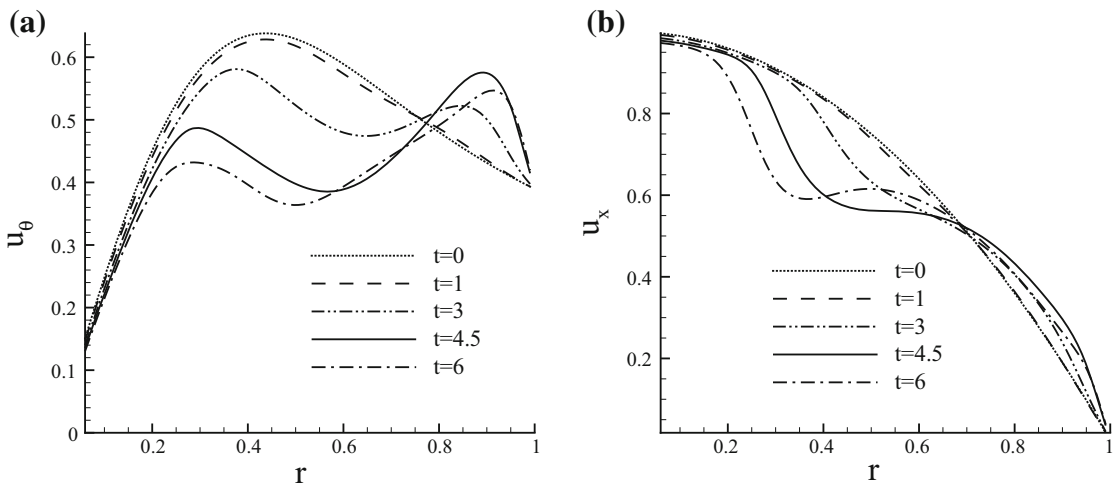

Fig. 8 Development of the perturbed **a** azimuthal velocity u_θ and **b** axial velocity u_x, averaged in the azimuthal and axial directions

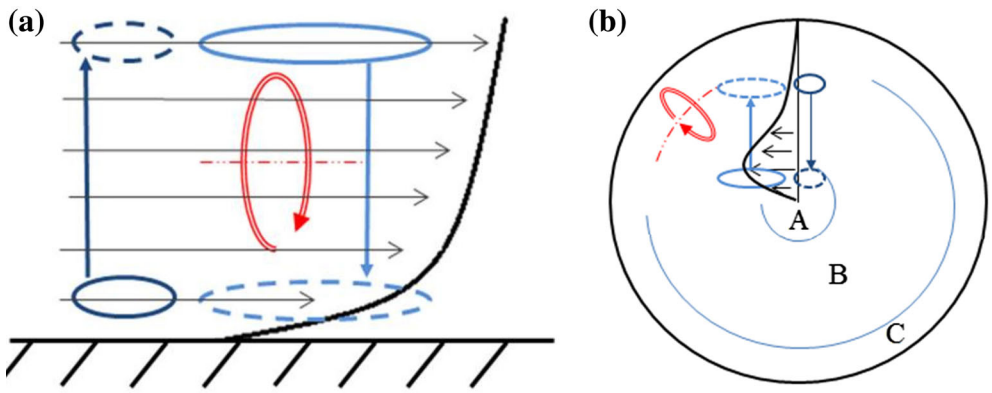

Fig. 9 Diagrams showing the lift-up mechanisms in **a** the $x - r$ plane and **b** the $\theta - r$ plane. The *arrows* show the motion of high- and low-velocity streaks. *A*, *B* and *C* denote the three regions of the domain

is the vorticity dominated region in the centre of the pipe, C is the axial shear flow dominated region near the wall boundary, and B is the region between A and C where the axial vorticity from the vortex and the axial velocity from the pipe flow interact (Fig. 9b).

A lift-up-stretch mechanism, referred to as (I), is sketched in Fig. 9a. This process originates from an axial vorticity disturbance, which acts to stir the axial velocity and generates low-speed and high-speed axial velocity streaks around regions B and C. Region A is far from the boundary and less affected in this mechanism. These streaks are stretched by the gradient of the base azimuthal velocity (see Fig. 4a) to tilt in the azimuthal direction and subsequently generate azimuthal vorticity. The transformation of perturbations in this mechanism can be described as

$$\tau_x \rightarrow u_x \rightarrow \tau_\theta$$

where τ_x and τ_θ are the axial vorticity and azimuthal vorticity, respectively. The first and second steps of this mechanism rely on the radial gradients of the axial and azimuthal base flow components, respectively.

The azimuthal vorticity generated in mechanism (I) induces another lift-up-stretch mechanism, denoted as (II) in the following. From Fig. 9b, it is seen that an azimuthal perturbation vorticity rotates high-speed base azimuthal velocity streaks to the boundary and low-speed base azimuthal velocity streaks towards the centre. These azimuthal velocity streaks are stretched by the gradient of the base axial velocity to tilt in the axial direction and subsequently generate axial vorticity (see Fig. 4b). The transformation of perturbations in this mechanism can be denoted as

$$\tau_\theta \rightarrow u_\theta \rightarrow \tau_x$$

The first and second steps of this mechanism rely on the radial gradients of the azimuthal and axial base velocity components, respectively.

The combination of the two mechanisms forms a complete amplification cycle and induces instability: an initial axial vorticity perturbation is amplified by mechanism (I) to generate azimuthal vorticity, which is subsequently amplified by mechanism (II) to generate axial vorticity. It is noticed that the combination of the two mechanisms occurs in region B, where the vortex and pipe flow interact since the gradients of both the axial velocity from the pipe flow and the azimuthal velocity from the vortex flow are reasonably high. This argument explains the distribution of the most unstable mode, which is mainly located in region B (see Fig. 4), and becomes more radially concentrated as q or R increases—otherwise the perturbation axial velocity will be over tilted and cannot be effectively converted to perturbation azimuthal vorticity. These two mechanisms induce radial mixing of the azimuthal and axial velocity components, as has been observed in both linear and nonlinear studies (see Figs. 4, 8).

These mechanisms can be also used to explain the decay of perturbations after nonlinear saturation observed in the DNS. The motions associated with mechanisms (I) and (II) cause the axial and azimuthal flow components in region B to be continually mixed and, over a long enough time period, the radial gradient of the flow does not support instability any more. The vorticity in the core region A is less affected because the unstable mode is mostly concentrated in the region B. Therefore the instability effectively suppresses the vorticity outside the vortex core but does not reach the core region.

It is worth noting that there is another mechanism, known as the anti-lift-up effect (III), occurring in the vortex flow outside the vortex core (in B and C) and transferring azimuthal velocity perturbations to azimuthal

vorticity perturbations. This mechanism is caused by a local Coriolis force and is related to the non-normality of the continuous spectrum of a vortex [13,14]. From the transformation of perturbation forms, it is noticed that the combination of the first step of (II) and (III) also forms a cycle, but this cycle does not generate any instabilities: both of them acting on the Lamb–Oseen vortex flow, which is asymptotically stable.

8 Conclusion

This work investigates the interaction of a vortex flow and a pipe flow, modelled as the Lamb–Oseen vortex and the Poiseuille flow, respectively. A relatively small Reynolds number $Re = 1{,}000$ is adopted. The combined flow is homogeneous in the axial direction, and therefore supports a Fourier decomposition in the axial direction in stability studies.

In asymptotic stability analyses, it is revealed that the combined flow becomes increasingly unstable at larger values of the swirling strength q, and the flow is asymptotically stable at $q \leq 0.2$. A swirling strength $q = 1$ is chosen as a typical case for detailed studies. It is observed that the globally most unstable mode appears at vortex radius $R = 0.39$, axial wavenumber $k = 5.1$ and azimuthal wavenumber $m = 4$, with energy concentrating outside the vortex core. The distribution of the unstable mode suggests that the instability is associated with radial convection of the base flow and the stretching effect.

Then the most unstable mode is used as the initial perturbation to disturb the model base flow in DNS. From this nonlinear evolution of the most unstable mode (leading mode), it is observed that the magnitude of the perturbation reduces after the nonlinear saturation. Further investigation of the higher harmonics of the leading modes shows that all the higher harmonics experience similar development history. Inspecting the development of the base mode (with axial wavenumber zero), it is noticed that the perturbation induces a sharp drop of the base mode energy, followed by a mild linear decay, and the transfer of these two trends occurs at the time point that the leading mode reaches maxima. From the contours of axial velocity and axial vorticity, it is clarified that the development of the perturbations suppresses the vorticity in the region outside the vortex core, decouples the vortex and the pipe flow, stabilises the combined flow and subsequently induces decay of perturbations. The generation and decay of such perturbations in the form of velocity streaks accompanied by vorticity pairs have been observed in an experimental study of pipe flow [26], while a similar vortex-induced instability has been reported in a plane shear flow [27].

The growing-decay development of the perturbations is explained as a combination of two lift-up-stretch mechanisms in the model flow. The two mechanisms occur in the region between the vortex core and the boundary (B in Fig. 9), and amplify perturbations through lift-up and stretching, both of which rely on the radial gradient of the base azimuthal and axial velocity components. The mixing of azimuthal velocity in this region owing to the development of the instability eventually leads to the suppression of vorticity, which effectively breaks the instability mechanism.

References

1. Burnham, D.C., Hallock, J.N.: Measurement of wake vortices interacting with the ground. J. Aircr. **42**, 1179–1187 (2005)
2. Harvey, J.K., Perry, F.J.: Flowfield produced by trailing vortices in the vicinity of the ground. AIAA J. **9**, 1659–1660 (1971)
3. Rusak, Z., Wang, S., Whiting, C.H.: The evolution of a perturbed vortex in a pipe to axisymmetric vortex breakdown. J. Fluid Mech. **366**, 211–237 (1998)
4. Rusak, Z., Wang, S., Xu, L., Taylor, S.: On the global nonlinear stability of a near-critical swirling flow in a long finite-length pipe and the path to vortex breakdown. J. Fluid Mech. **712**, 295–326 (2012)
5. Schmid, P.J., Henningson, D.S.: Stability and Transition in Shear Flows. Springer, New York (2001)
6. Mao, X., Sherwin, S.J.: Continuous spectra of the Batchelor vortex. J. Fluid Mech. **681**, 1–23 (2011)
7. Barkley, D., Blackburn, H.M., Sherwin, S.J.: Direct optimal growth analysis for timesteppers. Int. J. Numer. Methods Fluids **57**, 1435–1458 (2008)
8. Khorrami, M.R.: On the viscous modes of instability of a trailing line vortex. J. Fluid Mech. **225**, 197–212 (1991)
9. Bagheri, S., Schlatter, P., Schmid, P., Henningson, D.: Global stability of a jet in crossflow. J. Fluid Mech. **624**, 33–34 (2009)
10. Drazin, P., Banks, W.H.H., Zaturska, M.B.: The development of long's vortex. J. Fluid Mech. **286**, 359–377 (1995)
11. Batchelor, G.K.: Axial flow in trailing line vortices. J. Fluid Mech. **20**, 645–658 (1964)
12. Saffman, P.G.: Vortex Dynamics. Cambridge University Press, Cambridge (1992)
13. Antkowiak, A., Brancher, P.: On vortex rings around vortices: an optimal mechanism. J. Fluid Mech. **578**, 295–304 (2007)
14. Mao, X., Sherwin, S.J.: Transient growth associated with continuous spectra of the Batchelor vortex. J. Fluid Mech. **697**, 35–59 (2012)
15. Ellingsen, T., Palm, E.: Stability of linear flow. Phys. Fluids **18**, 487–488 (1975)
16. Landahl, M.T.: Wave breakdown and turbulence. SIAM J. Appl. Math. **28**, 735–756 (1975)

17. Yoshida, Y., Kawamura, T.: Numerical Simulation of the Transition Flow in the Smooth Pipe. Natural Science Report, Ochanomizu University (2013)
18. Broadhurst, M.S.: Vortex Stability and Breakdown: Direct Numerical Simulation and Stability Analysis Using BiGlobal and Parabolised Formulations. Ph.D. Thesis, Department of Aeronautics, Imperial College London (2007)
19. Blackburn, H.M., Barkley, D., Sherwin, S.J.: Convective instability and transient growth in flow over a backward-facing step. J. Fluid Mech. **603**, 271–304 (2008)
20. Heaton, C.J., Peake, N.: Algebraic and exponential instability of inviscid swirling flow. J. Fluid Mech. **565**, 279–318 (2006)
21. Hussain, F., Pradeep, D.S., Stout, E.: Nonlinear transient growth in a vortex column. J. Fluid Mech. **682**, 304–331 (2011)
22. Heaton, C.J.: Centre modes in inviscid swirling flows and their application to the stability of the Batchelor vortex. J. Fluid Mech. **576**, 325–348 (2007)
23. Blackburn, H.M., Sherwin, S.J.: Formulation of a Galerkin spectral element–Fourier method for three-dimensional incompressible flows in cylindrical geometries. J. Comput. Phys. **197**(2), 759–778 (2004)
24. Mao, X., Sherwin, S.J., Blackburn, H.M.: Non-normal dynamics of co-rotating vortex pairs. J. Fluid Mech. **701**, 430–459 (2012)
25. Mao, X., Blackburn, H.M., Sherwin, S.J.: Optimal inflow boundary condition perturbations in steady stenotic flows. J. Fluid Mech. **705**, 306–321 (2012)
26. Philip, J., Cohen, J.: Formation and decay of coherent structures in pipe flow. J. Fluid Mech. **655**, 258–279 (2000)
27. Sengupta, T.K., De, S., Sarkar, S.: Vortex-induced instability of an incompressible wall-bounded shear layer. J. Fluid Mech. **493**, 277–286 (2003)